PCCP

Accepted Manuscript

ROYAL SOCIETY OF CHEMISTRY

www.rsc.org/pccp

Coverage Dependent Water Dissociative Adsorption on Fe(110) from DFT Computation

*Shaoli Liu,[a,b,c] Xinxin Tian,[a,b,c] Tao Wang,[d] Xiaodong Wen,[a,b] Yong-Wang Li,[a,b] Jianguo Wang,[a,b] Haijun Jiao[a,d]**

a) State Key Laboratory of Coal Conversion, Institute of Coal Chemistry, Chinese Academy of Sciences, Taiyuan, 030001, China; b) National Energy Center for Coal to Liquids, Synfuels China Co., Ltd, Huairou District, Beijing, 101400, China; c) University of Chinese Academy of Sciences, No.19A Yuquan Road, Beijing, 100049, PR China; d) Leibniz-Institut für Katalyse e.V. an der Universität Rostock, Albert-Einstein Strasse 29a, 18059 Rostock, Germany. E-mail: haijun.jiao@catalysis.de

Abstract: Using density functional theory calculations and *ab initio* atomistic thermodynamics, H_2O adsorption and dissociation on the Fe(110) *p*(4×4) surface at different coverage have been computed. At the lowest coverage, the adsorbed H_2O, OH, O and H species can migrate easily on the surface. For $(H_2O)_n$ adsorption, H_2O molecules donating H atoms for H-bonding adsorb more strongly than those accepting H atoms for H-bonding. Monomeric H_2O dissociation is favored both thermodynamically and kinetically. On *n*O pre-covered Fe(110) surfaces (*n* = 1-8), H_2O dissociation is accessible for *n*O+H_2O (*n* = 1-7) both kinetically and thermodynamically, while H_2O desorption instead of dissociation occurs at *n* = 8. With the increased number of surface O atoms, H_2 dissociative adsorption energies vary in a narrow range for *n* = 1-4 and decreases for *n* = 5-7, while at *n* = 8, the surface does not adsorb H_2. At low OH coverage (*n* = 2, 4), OH groups are perpendicularly adsorbed without H-bonding, while for *n* ≥ 6, adsorbed OH groups are linearly arranged and stabilized by H-bonding. The maximal OH coverage (*n* = 12) is 0.75 ML and the reasonable O coverage (*n* = 7) is 0.44 ML, in line with the experiment. The calculated desorption temperatures of H_2O and H_2 agree well with the available experimental data. These results provide fundamental insights into water-involved reactions catalyzed by iron and interaction mechanisms of water interaction with metal surfaces.

Keywords: DFT, Fe(110) surface, H_2O adsorption and dissociation, hydrogen bonding, thermal desorption

1. Introduction

Water covers almost all solid surfaces under ambient condition. Water and metal interaction plays an important role in many aspects of scientific and technological processes.[1] The interaction of water with iron surfaces has been the subject of wide academic and industrial interests for decades, such as in water-gas shift (WGS) reaction and Fischer-Tropsch synthesis (FTS), and understanding the initial stage of the water adsorption and dissociation on iron surfaces is of essential importance. It is necessarily noted the reduction process of iron oxides by hydrogen, which is tightly related with water adsorption and dissociation on iron surfaces, remains elusive and challenging.

Using ultraviolet photoelectron spectroscopy, Dwyer *et al*.,[2] investigated H_2O adsorption on the clean and oxidized Fe(110) surfaces, and found molecular adsorption at 160K and surface hydroxyl groups at 225K. At 360K, H_2 desorption from the initially clean Fe(110) surface and H_2O desorption from the oxidized Fe(110) surface were observed. The oxygen coverage on the Fe(110) surface is approximately 0.4 monolayer (ML) and additional H_2O exposure hydroxylates the surface layer. Pirug *et al*.,[3] found that oxidation/penetration initiates at oxygen coverage of 0.4-0.5 ML on the Fe(110) surface. Baró *et al*.,[4] studied H_2O adsorption on the Fe(110) surface using electron energy loss spectroscopy at 130K, and found that H_2O molecules are dissociatively adsorbed resulting in surface hydroxyl species at low exposure (0.2 L), while molecularly adsorbed and form intermolecular H-bonding at high exposure. They found that thermal processing of adsorbed H_2O forms an oxygen over-layer and the adsorbed oxygen atoms have linear arrangement at high temperature.

Theoretically, Eder *et al*.,[5] showed that at low coverage H_2O adsorption on the Fe(110) surface slightly prefers the top site, and H_2O dissociation is barrier-less and the formed surface H atom and OH group are located at the three-fold hollow sites. However, the barrier-less process is contrary to the observation from ultraviolet photoelectron spectroscopy by Dwyer *et al*.[2]

In contrast to the Fe(100) surface which has attracted broad experimental and theoretical interests,[5-14] there are much less reports about H_2O adsorption and dissociation on the Fe(110) surface, although the Fe(110) surface is energetically more stable and also dominantly exposed on the crystal surface than the Fe(100) surface.[15]

As our ongoing interests in understanding the interaction of H_2O with iron surfaces, we carried out systematic analysis into H_2O adsorption and dissociation on the Fe(110) surface. We mainly focus on the preferred adsorption sites; coverage dependent adsorption structures; surface oxygen mediated H_2O dissociation as well as desorption of H_2O and H_2 molecules. This enables a direct comparison of H_2O adsorption between the Fe(110) and Fe(100) surfaces from our recent study.[16]

2. Methods and Models

(a) Method: All calculations were performed with the plane wave based pseudo-potential code in Vienna ab initio simulation package (VASP).[17,18] The electron-ion interaction is described with the projector augmented wave (PAW).[19,20] The exchange and correlation energies are described using the spin-polarized generalized gradient approximation and Perdew-Burke-Ernzerhof functional (GGA-PBE).[21] To enable direct and systematic comparison, we used the same parameters as in our previous study on H_2O adsorption on the Fe(100) surface,[16] i.e.; a cutoff energy of 400 eV and the Gaussian electron smearing method with σ = 0.20 eV for energies with errors due to smearing of less than 1meV per unit cell; and the convergence criteria of forces and energies of 0.02 eV/Å and 10^{-4} eV. All transition state structures were estimated using the climbing image nudged elastic band method (CI-NEB).[22] For each optimized stationary point vibrational analysis was performed at the same level of theory to determine its nature, either minimum or saddle point. The lattice parameters were calculated using the body-centered cubic (bcc) unit cell and its reciprocal space is sampled with a 15×15×15 *k*-point grid generated automatically using the Monkhorst-Pack method.[23] The computed lattice constant (2.835 Å) and magnetic moment (2.226 μ_B) are close to the experimental values (2.866 Å[24] and 2.22 μ_B[25]). Since the adsorption and intermolecular interaction of H_2O molecules are influenced significantly by the weak interaction, like H-bonding,[26] we carried out long-range dispersion correction for van der Waals interaction for H_2O adsorption

on the Fe(110) surface using the semi-empirical GGA-type functional (PBE-D2) by Grimme.[27] It is reported that dispersion correction from PBE-D2 functional generally overestimates adsorption energies.[28-30] In our study[16] we also found that such correction overestimates the adsorption energies and desorption temperature of H_2O and H_2 on the Fe(100) surface (Table S1). Since PBE-D2 overestimates the adsorption energies and desorption temperature of H_2O and H_2 on the Fe(110) surface, we used the pure PBE energies for our comparison and discussion.

(b) Model: For the Fe(110) surface, a periodic slab with a vacuum region in 15 Å width was used to separate the periodically repeated slabs. To choose a reasonable slab model for H_2O adsorption, we tested the effects of the number of relaxation layers, *k*-points and surface size on H_2O adsorption energy (Table S2). On the basis of these tests, surface structure relaxation and total energy calculation were performed with the 3×3×1 Monkhorst-Pack *k*-point sampling. For the *p*(4×4) surface size, a four-layer model containing 64 Fe atoms was used, where the first two layers including adsorbates were relaxed and the bottom two layers were fixed. The top and side views and possible adsorption sites of the Fe(110) surface are shown in Figure. 1.

(**Figure 1**)

The adsorption energy was defined in equation 1, where $E_{X/slab}$ is the total energy of the slab with adsorbates in its equilibrium geometry, E_{slab} is the total energy of the clean surface, and E_X is the energy of the free adsorbates in gas phase. Therefore, the more negative the E_{ads}, the stronger the adsorption. The desorption energy E_{des} is defined as the negatives of the E_{ads} ($E_{des} = -E_{ads}$). It is noted that the reported adsorption energies do not include the corrections of zero-point energies (E_{ads}), since they have negligible effect on the trends of the reactions on iron surfaces[31,32] and iron carbide surfaces.[33]

$$E_{ads} = E_{X/slab} - E_{slab} - E_X \quad (1)$$

The activation barrier E_a and the reaction energy E_r are defined in equations 2 and 3; where E_{IS}, E_{TS}, and E_{FS} are the energies of the corresponding initial (IS), transition (TS) and final (FS) states, respectively.

$$E_a = E_{TS} - E_{IS} \quad (2)$$

$$E_r = E_{FS} - E_{IS} \quad (3)$$

To study the stabilizing factor of the surface oligomers, we defined the sequential hydrogen bonding energy ($E_{H\text{-}bond}$, Eq. 4) of the latest H_2O molecule in a water oligomer, and the adsorption energy ($E_{H2O/M}$, Eq. 5) between the latest H_2O and the surface. In Eq. 4 and Eq. 5, $E_{(H2O)n}$ and $E_{(H2O)n-1}$ is the single-point energy of an oligomer $[(H_2O)_n]$ and the species except the latest water $[(H_2O)_{n-1}]$ in gas phase having the geometries adsorbed on the surface, respectively; $E_{H2O/Fe}$ and E_{H2O} are the single-point energies of the latest H_2O molecule on the surface and in gas phase having geometry adsorbed on the surface, and E_{slab} corresponds to the single-point energy of the slab after the adsorbates adsorbed.

$$E_{H\text{-}bond} = E_{(H2O)n} - E_{(H2O)n-1} - E_{H2O} \quad (4)$$

$$E_{H2O/M} = E_{H2O/Fe} - E_{H2O} - E_{slab} \quad (5)$$

(c) Atomistic thermodynamics: Atomistic thermodynamics[34,35] is a convenient tool to study reactions under specific condition.[36-40] Since this is the same procedure used in our previous study,[16] the detailed description can be found in our previous work or Supporting Information.

3. Results and discussions

3.1 Adsorption of H, O, OH and H_2O on Fe(110): The adsorption of H, O, OH and H_2O on the Fe(110) surface at the top (**T**), long-bridge (**LB**), short-bridge (**SB**) and 3-fold hollow (**3FH**) sites by considering different initial adsorption configurations was computed. The adsorption energy and structure parameters of the species along with the available literature data are listed in Table 1, and the detailed structural parameters in all adsorption sites are listed in Table S3. The most stable configurations of the species are given in Figure 1.

(**Table 1**)

For a H atom, the most stable adsorption configuration is at the **3FH** site (-0.76 eV) as reported in the previous studies,[5,41] while Cremaschi *et al*.[42] reported the most stable position to be the **LB** site. Our second stable adsorption site is the **LB** site (-0.71 eV), while the **SB** site is very less stable (-0.59 eV) and H adsorption on the **T** site does not exist. The Fe-H distances at the **3FH** site are 1.787, 1.790 and 1.792 Å. The adsorbed H atom can move easily on the surface from one **3FH** site to another **3FH** site through the **SB** site via barrier of 0.17 eV.

For an O atom, the adsorption configurations at the **LB** and **3FH** sites have the same adsorption energy (-3.43 eV), and they are much more stable than those at the **SB** and **T** sites (-2.94 and -1.77 eV, respectively) and the Fe-O distances at the **LB** site are 1.846, 1.846, 2.166 and 2.221 Å. This is in agreement with the study of Baró *et al*.,[4] where they found that O atom only occupies the **LB** site at room temperature. Other studies[5,43,44] also found that the **LB** site is energetically most stable for O atom adsorption. The adsorbed O atom can transfer easily through the **SB** site via barrier of 0.49 eV from one **LB** site to another **LB** site.

For an OH group, the most stable adsorption configurations is at the **3FH** site with adsorption energy of -4.28 eV, and it is much more stable than those at the **SB** and **T** sites (-3.95 and -3.45 eV, respectively) and the Fe-O distances at the **3FH** site are 2.002, 2.006, 2.151 and 2.647 Å. At the **3FH** site, the O-H bond is perpendicular to the iron surface. It is also noted that the adsorption configuration at the **LB** site is not stable and goes to the **3FH** site directly during the optimization. Eder *et al*.,[5] found that the **LB** site is energetically most stable for OH group adsorption. The OH group can transfer from one **3FH** site to another **3FH** site through the **SB** site via barrier of 0.33 eV.

For a H_2O molecule, the most stable adsorption configuration is at the **T** site (-0.38 eV) with H_2O molecule parallel to the iron surface and the Fe-O distance of 2.183 Å. The computed H_2O migration barrier from one **T** site to another **T** site via the **SB** site is only 0.10 eV. Therefore, all four surface species can migrate easily on the Fe(110) surface; and this will affect the high coverage adsorption configuration.

3.2 Aggregation of water molecules on Fe(110): Due to the interaction of H_2O with surface iron atoms and H-bonding among adsorbed H_2O molecules, we used sequential adsorption to find the most stable adsorbed H_2O clusters on the iron surface. For example, one H_2O molecule was added to the previous most stable one for getting the next most stable one after considering both interactions. The most stable adsorption configurations of H_2O clusters on the Fe(110) surface are shown in Figure 2. The computed adsorption energies and selected bond parameters are listed in Table S4.

(**Figure 2**)

For $(H_2O)_2$ adsorption, one H_2O molecule, which is the H donor for H-bonding, adsorbs at the **T** site with Fe-O distance of 2.080 Å, which is shorter than that of one H_2O adsorption (2.183 Å). The second H_2O molecule, which is the H acceptor for H-bonding, stands over the **T** site of the surface Fe atom and has very long Fe-O distance (3.088 Å). The H-bonding distance is 1.639 Å. The adsorption energy of $(H_2O)_2$ is -0.98 eV, higher than twice of one H_2O adsorption (-0.76 eV). The sequential H-bonding energy is -0.22 eV, and the adsorption energy of the second adsorbed H_2O molecule is -0.15 eV, indicating that H-bonding is dominant.

The adsorption of $(H_2O)_3$ does not forms a cyclic geometry. The middle H_2O molecule, which provides both H atoms for H-bonding, adsorbs at the **T** site with Fe-O distance of 2.019 Å, which is shorter than those of H_2O and $(H_2O)_2$ adsorption (2.183 and 2.080 Å, respectively). The other two H_2O molecules, which are the H acceptors for H-bonding, stand over the **T** sites of the surface Fe atoms with very long Fe-O distance (3.037 and 3.059 Å). The H-bonding distances are 1.693 and 1.697 Å, longer than that in $(H_2O)_2$ adsorption (1.639 Å). The adsorption energy is -1.53 eV, higher than three-fold of one H_2O adsorption (-1.14 eV). The sequential H-bonding energy is -0.08 eV, and the adsorption energy of the third adsorbed H_2O molecule is -0.16 eV.

The lowest energy structure of $(H_2O)_4$ is star-like, in contrast to the cyclic gas phase structure. This star-like structure can be considered as the adsorption of the fourth H_2O molecule to the $(H_2O)_3$ structure. In $(H_2O)_4$, the central H_2O molecule, which provides both H atoms for H-bonding, binds tightly with the surface Fe atom (2.152 Å) at the **T** site; and the other two H_2O molecul-

es, which are the H acceptors for H-bonding, stand over the **T** site of the surface Fe atoms with very long Fe-O distances (3.032 and 3.054 Å). The H-bonding distances are 1.665 and 1.669 Å. The fourth H_2O molecule, which provide one H atom for H-bonding (1.692 Å) to the central H_2O molecule, adsorbs also tightly to the surface Fe atom at the **T** site with short Fe-O distance (2.106 Å). The adsorption energy is -2.12 eV, higher than four-fold of one H_2O adsorption (-1.52 eV). The sequential H-bonding energy is -0.43 eV, and the adsorption energy of the fourth adsorbed H_2O molecule is -0.40 eV. This reveals that both interactions dominate the aggregation of the fourth H_2O molecule in the adsorbed $(H_2O)_4$ cluster.

There are three adsorption structures for $(H_2O)_5$. The most stable one $(H_2O)_{5-t1}$ has a four-membered ring with an exocyclic H_2O unit and can be deduced from the star-like $(H_2O)_4$. As discussed above, the two H_2O molecules which provide H atoms for H-bonding adsorb stably at the **T** sites of surface Fe atoms with shorter Fe-O distances (2.064 and 2.154 Å); and the rest three H_2O molecules which accept H atoms for H-bonding stand over the **T** sites with longer Fe-O distances (3.134, 3.319 and 3.324 Å). There are four shorter (1.637, 1.710, 1.754 and 1.772 Å) and one longer (2.001 Å) H-bonding. The adsorption energy is -2.65 eV, higher than five-fold of single H_2O adsorption (-1.90 eV). The sequential H-bonding energy is -0.17 eV, and the adsorption energy of the fifth adsorbed H_2O molecule is only -0.11 eV. In addition, we computed two monocyclic $(H_2O)_5$ structures with H-bonding, $(H_2O)_{5-t2}$ and $(H_2O)_{5-t3}$. In $(H_2O)_{5-t2}$, one H_2O provides double H atoms for H-bonding; and one H_2O works as double H-acceptor for H-bonding and the rest three H_2O molecules are both H-donor and acceptor for H-bonding. In $(H_2O)_{5-t3}$, each H_2O molecule works as both H-donor and acceptor for H-bonding. The computed adsorption energies of $(H_2O)_{5-t2}$ and $(H_2O)_{5-t3}$ are -2.60 and -2.57 eV, close to that of $(H_2O)_{5-t1}$, indicating rather small energy difference despite of larger structure changes.

For $(H_2O)_n$ (n = 1-5), the most stable adsorption configurations can be deduced step by step; where the adsorbed H_2O molecules providing H atom for H-bonding adsorb more tightly with the surface atoms than those standing over the surface and accepting H for H-bonding. On the basis of this adsorption moiety we explored the structures of $(H_2O)_6$. Starting from $(H_2O)_{5-t1}$ and $(H_2O)_{5-t2}$, we added the sixth H_2O molecule to the tightly adsorbed H_2O molecule, which provide both H atoms for H-bonding, and the resulting structures are $(H_2O)_{6-t1}$ and $(H_2O)_{6-t2}$, and both structures have three shorter and three longer Fe-O distances. The computed adsorption energy of $(H_2O)_{6-t1}$ and $(H_2O)_{6-t2}$ is -3.10 and -3.16 eV, respectively.

Intuitively we computed a hexagonal structure with alternating shorter (2.174, 2.183, and 2.199 Å) and longer (3.064, 3.082, and 3.137 Å) Fe-O distance in a chair form, $(H_2O)_{6-t3}$, and each H_2O molecule is both H-donor and acceptor for H-bonding. There are shorter (1.554, 1.569, and 1.591 Å) and longer (1.820, 1.855, and 1.856 Å) H-bonding. For comparison we computed the gas phase structure of a chair-like hexagonal $(H_2O)_6$, which has alternating shorter (1.569, 1.581, 1.608 Å) and longer (1.819, 1.843, and 1.881 Å) H-bonding. The computed adsorption energy of $(H_2O)_{6-t3}$ is -3.23 eV, higher than six-fold of single H_2O adsorption (-2.28 eV). It is also noted that $(H_2O)_{6-t3}$ is more stable than $(H_2O)_{6-t1}$ and $(H_2O)_{6-t2}$. Experimentally, Baró *et al.*,[4] proposed a cyclic hexamer of water molecules on the Fe(110) surface.

On the basis of the hexacyclic $(H_2O)_{6-t3}$, we computed the adsorbed structures of $(H_2O)_7$, $(H_2O)_8$, and $(H_2O)_{9-t1}$, where the last H_2O molecule has been added at the exocyclic site as H atom acceptor; and all these exocyclic H_2O molecules have longer Fe-O distances; and the adsorption energy of $(H_2O)_7$, $(H_2O)_8$, and $(H_2O)_{9-t1}$ is -3.80, -4.35 and -4.77 eV, respectively. In addition we also computed a second $(H_2O)_{9-t2}$ structure with a fused five-membered ring to the six-membered ring, and the adsorption energy is -4.92 eV, which is higher than that of $(H_2O)_{9-t1}$ by 0.15 eV.

Our computed results show that the most stable adsorption configuration can be deduced step by step for $(H_2O)_n$ (n = 1-5), and for $n \geq 6$, the stable configuration of the adsorbed water clusters is based on a hexagonal structure. Different from Fe(110) surface, the preferred configurations on Fe(100) surface are based either on four-membered or five-membered rings.[16]

3.3 H_2O dissociation on clean surface:

(a) Monomeric H_2O dissociation [$H_2O \rightarrow O + H_2(g)$]: On the basis of the most stable adsorbed H_2O structure at the **T** site, we

calculated H_2O dissociation into surface H and OH on the Fe(110) surface. The optimized structures of the IS, TS and FS are shown in Figure 3, and the structural parameters are listed in Table S5. The reaction barriers, the reaction energies and the structural parameters of the TS are shown in Table S6. The total reaction potential energy surfaces are shown in Figure 4.

(**Figures 3 and 4**)

In the transition state (**TS1**), the breaking O-H distance is 1.401 Å. In the final state, the adsorbed OH and H are at the **LB** and **3FH** sites, respectively. The energy barrier is 0.68 eV and the reaction is exothermic by 1.28 eV. For the dissociation of the surface OH group into surface O and H, the breaking O-H distance in the transition state (**TS2**) is 1.273 Å. In the final state (O+2H), the O and H atoms are located at the **3FH** sites. The computed dissociation barrier is 0.90 eV, and the dissociation is exothermic by 0.57 eV. It shows that the first dissociation barrier is larger than the adsorption energy, and the first dissociation step is adsorption controlled. Since the total dissociation is highly exothermic (-2.23 eV relative to H_2O(g) or -1.85 eV relative to H_2O(s)), H_2O dissociation on the Fe(110) surface should occur very easily. Starting from the co-adsorbed final state, the formation of H_2(g) is endothermic by 1.33 eV. However, the formation of O + H_2(g) is exothermic by 0.52 eV to H_2O(s) or by 0.90 eV to H_2O(g).

(b) Dimeric H_2O dissociation [$(H_2O)_2$ = O + H_2(g) + H_2O]: Stabilized by H-bonding, we are interested in the dissociation of $(H_2O)_2$. The optimized geometries for the stationary points of IS, TS, and FS are shown in the Supporting Information (Figure S1), and the bond parameters of these points are listed in Table S5. The dissociation barriers, dissociation energies, and critical bond distances of TS are given in Table S6. The total potential energy surfaces are shown in Figure 4. Since there are two differently adsorbed H_2O molecules, both dissociations are computed. For the dissociation of adsorbed $(H_2O)_2$, we consider two steps: (*i*) $(H_2O)_2 \rightarrow$ OH+H+H_2O and (*ii*) OH+H+$H_2O \rightarrow$ O+2H+H_2O.

In the first step, for the H_2O molecule with longer Fe-O distance, the barrier is 0.61 eV and the breaking O-H distance in the transition state (**TS3**) is 1.360 Å as well as the dissociation is exothermic by 0.89 eV. In the second step, the barrier is 0.57 eV and the breaking O-H distance in the transition state (**TS4**) is 1.403 Å as well as the dissociation is exothermic by 0.86 eV. For the dissociation of the H_2O molecule with shorter Fe-O distance, the barrier of the first step is 0.88 eV and the breaking O-H distance in the transition state (**TS3'**) is 1.294 Å as well as the dissociation is exothermic by 0.98 eV. In addition, we computed the competitive reaction, OH+H+$H_2O \rightarrow$ 2OH+2H. The dissociation barrier is 0.64 eV and the breaking O-H distance is 1.291 Å in the transition state (**TS5**) as well as the dissociation is exothermic by 1.11 eV. It shows that the co-adsorbed H_2O molecule can lower the barriers of H_2O dissociation, especially the barrier of OH dissociation.

(c) H_2O dissociation on O pre-covered surface: With the formation of gaseous H_2(g) from the surface, it is crucial to study H_2O adsorption and dissociation on O-pre-covered surface. On O pre-covered surface, H_2O dissociation is modeled with sequential increase of H_2O molecule after the formation of H_2(g), i.e.; *n*O + H_2O(g) $\rightarrow$ (*n+1*)O + H_2(g) (*n* = 1-8). The optimized structures for the stationary points of IS, TS and FS are given in the Supporting Information (Figure S2-S9); the bond parameters of IS and FS are given in Table S7. The dissociation barriers, dissociation energies and critical bond distances of TS are given in Table S8. The full potential energy surface is shown in Figure S10 and the selected energy profiles are shown in Figure 4.

The model starts with the co-adsorption of the adsorbed surface O and one gas phase H_2O(g). The computed adsorption energy of H_2O is -0.45 eV, which is slightly higher than that (-0.38 eV) on the clean surface. In the initial state O+H_2O(s), the H-bonding distance is 1.885 Å. There are three steps of H_2O dissociation: O assisted dissociation into OH+OH, one OH of OH+OH further dissociates into O+H+OH, and then direct O+H+OH dissociates into 2O+2H. In the first step, the barrier is 0.40 eV, which is very close to the adsorption energy of H_2O(g), and the reaction is exothermic by 0.38 eV. In the transition state **TS6**, the breaking O-H distance is 1.350 Å. The reverse reaction, 2OH = O+H_2O(s), which is also the disproportionation reaction, has energy barrier of 0.78 eV and is endothermic by 0.38 eV. For the dissociation of OH+OH into O+H+OH, the barrier is 0.90 eV and the reaction is exothermic by 0.57 eV. In the transition state **TS7**, the breaking O-H distance is 1.295 Å. For the further dissociation of O+H+OH into

2O+2H, the barrier is 0.95 eV and the reaction is exothermic by 0.29 eV. In the transition state **TS8**, the breaking O-H distance is 1.326 Å. Desorption of H_2(g) needs energy of 0.98 eV. As shown in Figure 4, the overall reaction for 2O+H_2(g) is exothermic by 0.26 eV starting from O+H_2O(s) or by 0.71 eV relative to H_2O(g).

For the co-adsorption of the adsorbed surface 2O and one gas phase H_2O [2O+H_2O(g)], the adsorption energy of the third H_2O(g) is -0.31 eV, which is slightly lower than that on the clean surface (-0.38 eV) and one O-pre-covered surface (-0.45 eV). The barrier of 2O+H_2O(s) dissociation into O+2OH is 0.41 eV and the reaction is exothermic by 0.48 eV. The breaking O-H distance in the transition state **TS9** is 1.384 Å. For the dissociation of O+2OH into 2O+H+OH, the barrier is 1.01 eV and the reaction is exothermic by 0.46 eV. The breaking O-H distance in the transition state **TS10** is 1.300 Å. For the further dissociation of 2O+H+OH into 3O+2H, the barrier is 1.02 eV and the reaction is exothermic by 0.22 eV. The breaking O-H distance in its transition state **TS11** is 1.329 Å. Desorption of H_2(g) needs energy of 0.93 eV. As shown in Figure S10, the overall reaction for 3O+H_2(g) is exothermic by 0.23 eV starting from 2O+H_2O(s) or by 0.54 eV relative to H_2O(g).

Since further H_2O dissociations on *n*O pre-covered Fe(110) surfaces (*n* = 3-8) have similar potential energy surface patterns as found for that on O and 2O pre-covered surfaces (Figure S10), we show their trends for general discussion and comparison (Figure 5). It shows that the adsorption energies of H_2O, E_{ads} [*n*O+H_2O(g) = *n*O+H_2O(s)], increase gradually with the increase of the adsorbed surface O atoms; and the largest adsorption energy is found for *n* = 7 (-0.72 eV), while that for *n* = 8 is only -0.33 eV. The first step *n*O+H_2O → (*n-1*)O+2OH has always lower energy barrier (E_{a1}, 0.32 - 0.58 eV) for *n* = 3-7. For *n* = 8, the barrier of the first step dissociation of the ninth H_2O is 0.79 eV, and this step is endothermic by 0.43 eV. Since the adsorption energy (0.33 eV) of the ninth H_2O is much lower than the first step dissociation barrier, desorption instead of dissociation should be favored. This indicates that for O coverage with eight surface O atoms (0.5 ML), the ninth H_2O can adsorb but does not dissociate.

(**Figure 5**)

For the following OH dissociation steps, (*n-1*)O+2OH = *n*O+H+OH and *n*O+H+OH = (*n+1*)O+2H, the dissociation barriers (E_{a2} and E_{a3}) are in the range of 0.90-1.10 eV for *n* = 3-6, while 1.31 and 1.19 eV for *n* = 7 as well as 1.28 and 2.09 eV for *n* = 8. For *n* = 6, the OH dissociation is exothermic by 0.19 eV, while endothermic by 0.12 and 0.83 eV for *n* = 7 and 8, respectively. It reveals that the Fe(110) surface can have seven oxygen atoms (0.44 ML) and therefore, H_2O dissociative adsorption into surface O and H atoms is feasible for *n* = 1-7 (ML ≤ 0.44) both kinetically and thermodynamically. This expected surface O coverage of 0.44 ML is indeed in agreement with the experimental observations.[2,3]

For the last step, (*n+1*)O+2H = (*n+1*)O + H_2(g), H_2 desorption energy varies in the range of 0.84-0.98 eV with the increased surface O atoms for *n* = 3-5, while H_2 desorption energy decreases with the increasing of O coverage for *n* = 6-7 (0.66 eV to 0.49 eV). For *n* = 8, H_2 desorption is exothermic by 0.39 eV, indicating that the surface fully covered by oxygen atoms does not adsorb H_2.

Compared with the previous studies on the Fe(100) surface,[16] H_2O dissociation on O-pre-covered Fe(110) surface is similar as that on the Fe(100) surface. On the Fe(100) surface, H_2O molecules can dissociate as long as the preferred free adsorption sites are available, on the Fe(110) surface, however, the largest O coverage is 0.44 ML (n = 7) and additional H_2O molecule can adsorb but does not dissociate.

3.4 High OH and O coverage: The most stable adsorption configurations of OH and O groups at different coverage are shown in Figure 6. It is found that the larger of the non-bonded O-O distance between two OH species the more stable of the adsorption configuration. For the most stable adsorption configuration of 2OH, both OH groups are perpendicularly adsorbed at the **LB** sites of the iron surface and the same is also found for the adsorption of 4OH (Figure 6a). In the most stable adsorption configuration of 6OH, two OH groups are perpendicularly adsorbed at the **LB** sites, while four OH groups are parallel adsorbed at the **SB** sites in a linear arrangement and each OH group acts as both H-donor and H-acceptor for H-bonding (1.596, 1.597 and 1.593 Å).

(**Figure 6**)

For the adsorption of 8OH (0.5 ML), there are two parallel lines of linearly arranged OH groups at the **SB** sites and each OH acts as both H-donor and H-acceptor for H-bonding. The distance of the H-bonding between the adjacent OH species is 1.601 Å, and the non-bonded O-O distance is 2.455 Å, which is the same as that of the Fe-Fe distance. Thermodynamically, the formation of 0.5 ML OH coverage is exothermic by 5.14 eV on the basis of eight gaseous H_2O molecules [$8H_2O(g) = 8OH(s) + 4H_2(g)$].

For the adsorption of 12OH (0.75 ML), there are three parallel lines of linearly arranged OH groups at the **SB** sites and each OH acts as both H-donor and H-acceptor for H-bonding. There are two H-bonding distances between the adjacent OH species (1.590 and 1.609 Å); and this difference is mainly due to the different O-H distances (1.000 and 1.004 Å) in one OH group and the different tilt angles (23.98 and 25.01°) of the OH species. However, the non-bonded O-O distance is the same as in case of 8OH (2.455 Å). Thermodynamically, the formation of 0.75 ML OH coverage is exothermic by 4.50 eV on the basis of twelve gaseous H_2O molecules [$12H_2O(g) = 12OH(s) + 6H_2(g)$].

By adding one more OH group on the surface, surface OH disproportionation takes place and forms H_2O for desorption [$2OH = O + H_2O(g)$], therefore, the largest OH coverage is 0.75 ML (n = 12). Nevertheless, we also tried to calculate the stable structure of 1 ML OH coverage (n = 16). Starting from a perfectly arranged surface structure, optimization results in the adsorption configuration of $6O+4OH+6H_2O$, where only two H_2O molecules adsorb at the Fe surface, and the other four H_2O molecules adsorb through the H-bonding to the surface adsorbed O atoms. After desorption of the two molecular adsorbed H_2O and also H_2O from OH disproportionation, the surface will have eight adsorbed O atoms (θ_O = 0.5 ML). It is also very interesting to note that the surface structure of the adsorbed O atoms and OH groups are in linear arrangement, where there are one line of four O atoms, one line of four OH groups as well as one line of two O atoms. This linear arrangement is also in agreement with the experimental observation at high temperature.[4]

The most stable adsorption configurations of O atom at different coverage are shown in Figure 6b. It is noted that our $p(4\times4)$ surface model is much larger than those from previous study[43] using $p(2\times2)$, $c(2\times2)$, $p(2\times1)$ and $p(1\times1)$ surface models. All adsorbed O atoms are at either the **LB** or **3FH** sites, and average O adsorption energy decreases as the increasing of the O coverage, in line with the results of Błoński *et al*.[43] At 0.25, 0.5 and 1 ML (n_O = 4, 8 and 16), however, our computed average adsorption energies (-3.40, -2.99 and -2.22 eV, respectively) are larger than those obtained using smaller surface models (-3.28, -2.77/-2.54 and -1.49 eV, respectively).[43] Due to the repulsive interaction of the adsorbed O atoms, the adsorbed surface structures for 6O, 8O and 12O do not show any regular and symmetrical patterns. It is noted that these results are obtained only using oxygen atom as reference and do not represent the results on the basis of H_2O dissociative adsorption.

There are significant differences in the adsorption of OH and O between Fe(110) and Fe(100) surfaces. On the Fe(100) surface,[16] the most stable adsorbed OH groups have H-bonding interaction and form a well-ordered linear structure at the bridge site from low to high coverage, and the average OH adsorption energy increases as the increasing of the OH coverage. While on the Fe(110) surface, the OH groups are separately and perpendicularly adsorbed and do not have H-bonding interaction at low coverage, and the average OH adsorption energy decreases as the increasing of the OH coverage. Considering the formation of gaseous H_2, it is thermodynamically possible to have 1 ML OH or 1 ML O coverage on the Fe(100) surface, although the formation of 1 ML O is kinetically hindered. While on the Fe(110) surface, the maximum surface OH coverage is 0.75 ML, and the largest O coverage is 0.44 ML.

3.5 Desorption of H_2O and H_2 on Fe(110): On the basis of our calculated stable adsorption states, we are interested in H_2O and H_2 desorption at different temperatures and certain pressure. On the basis of Gibbs free energy changes of the related reactions at different temperatures (Figure 7), one can estimate the temperatures for reaction and desorption. In our study on the Fe(100) surface[16] we found excellent agreement between theory and experiment in desorption temperatures of H_2O and H_2 from surface

OH disproportionation and dissociation under ultra-high vacuum condition. We therefore computed H_2O and H_2 desorption from the Fe(110) surface at 1.3×10^{-13} atm (or 1×10^{-10} Torr) for direct comparison with the experimental results.

(**Figure 7**)

In our study we computed H_2O desorption from adsorption and OH disproportionation (Figure 7a). For the desorption of stably adsorbed H_2O molecule [$H_2O(s) \rightarrow H_2O(g)$], the computed desorption temperature is 232K. Since the adsorption energy and first dissociation barrier of H_2O are in the same magnitude, the computed temperature at 232K should also represent the dissociation temperature to form surface hydroxyl groups due to the very strong thermodynamic driving force. This agrees with the observed 225K from ultraviolet photoelectron spectroscopy study,[2] where the adsorbed H_2O dissociates into surface hydroxyls.

For H_2O desorption from OH disproportionation [$2OH(s) \rightarrow O(s) + H_2O(g)$], the computed desorption temperature is at 333K, which is close to the observed 315K.[2] On O pre-covered surfaces, H_2O desorption temperatures are higher than that on the clean surface, apart from 2O and 8O pre-covered surfaces (Figure 7b).

For H_2 desorption from the clean surface [$2H(s) \rightarrow H_2(g)$], the computed desorption temperature is at 411K, which should represent the up limit value. That H_2 has higher desorption temperature than H_2O from OH disproportionation is also in agreement with the experimental observation from changing the temperature from 325 to 460K. For H_2 desorption from oxygen covered surfaces, desorption temperatures are lower than that from the clean surface (411K), indicating the easy desorption of the formed H_2 from H_2O dissociation (Figure 7c).

4. Conclusions

Coverage dependent H_2O adsorption and dissociation on the Fe(110) surface have been studied on the basis of periodic density functional theory calculations and ab initio atomistic thermodynamics. The main points can be summarized as following.

(a) On the clean surface at the lowest coverage, H atom prefers the three-fold hollow site, O atom at the long-bridge (**LB**) and three-fold hollow (**3FH**) sites has the same adsorption energy and OH group is perpendicularly located at the three-fold hollow (**3FH**) site as well as H_2O is located nearly parallel at the top (**T**) site. All these surface species can migrate easily on the surface, indicating their high surface mobility. The calculated desorption temperatures of H_2O and H_2 on the surfaces agree with the available experimental data.

(b) For the adsorption of $(H_2O)_n$ clusters (n = 1-9), both adsorption and H-bonding play the role in stabilizing and determining the cluster configurations. It is found that H_2O molecules which provide H atoms for H-bonding adsorb more tightly and strongly at the top sites of surface iron atoms than those which accept H atoms for H-bonding stand over surface iron atoms with longer Fe-O distances. For n = 1-5, the stable adsorption configurations can be deduced by stepwise H_2O adsorption by considering of adsorption and H-bonding, and both $(H_2O)_4$ and $(H_2O)_5$ have star-like structural patterns, while for $n \geq 6$, the stable configurations are based on a hexagonal structure, in agreement with the proposal from experiment. These results are different from the basic structures of $(H_2O)_n$ on the Fe(100) surface, where they are based either on four-membered rings or on five-membered rings.

(c) Monomeric H_2O dissociation is favored both thermodynamically and kinetically. The co-adsorbed H2O molecule can lower the barriers of water dissociation, especially the barrier of OH dissociation.

(d) On the O pre-covered surface (n_O = 1-8), the sequential adsorption energy of H_2O, E_{ads} [$nO+H_2O(g) = nO+H_2O(s)$], increases gradually with the increase of the adsorbed surface O atoms; and the largest adsorption energy is found for n = 7. The first step dissociation, $nO+H_2O \rightarrow (n-1)O+2OH$, is feasible for $nO+H_2O$ (n = 1-7, $\theta_O \leq 0.44$) both kinetically and thermodynamically and has always lower energy barrier. For n = 8, H_2O desorption rather than dissociation should occur. The expected O coverage (0.44 ML) is in perfect agreement with the experiment.

(e) On the O pre-covered surface, H_2 desorption energy, E_{des} [$(n+1)O+2H=(n+1)O+H_2(g)$], varies in a narrow range with the in-

creased number of surface oxygen atoms for n = 1-4 and decreases for n = 5-7, while for n = 8, the surface does not adsorb H_2.

(f) For OH adsorption at low coverage, the perpendicularly adsorbed OH groups prefer dispersion and do not form H-bonding for n = 1-4. For $n \geq 6$, several OH species can form the hydrogen bonding and linearly arranged structures. The average OH adsorption energy decreases as the increasing of the OH coverage. The maximum OH coverage is 0.75 ML (n = 12), there are three parallel lines of linearly arranged OH groups at the long-bridge (**LB**) sites and each OH acts as H-donor and H-acceptor for H-bonding. These aspects are different from that on the Fe(100) surface, where the adsorbed OH groups form linearly ordered structures and H-bonding from low to high coverage; and it is thermodynamically possible to have 1 ML OH.

These results provide fundamental insights into water-involved reactions catalyzed by iron particularly and our understanding of water interaction with metal surfaces generally.

Acknowledgment: This work was supported by the National Basic Research Program of China (no. 2011CB201406), the National Natural Science Foundation of China (no. 21273262&21273266), and the Chinese Academy of Science and Synfuels CHINA. Co., Ltd. We also acknowledge general financial support from the BMBF and the state of Mecklenburg-Vorpommern.

Electronic Supplementary Information (ESI) available: Adsorption energies and desorption temperature of H_2O and H_2 under some different conditions on Fe(110) surface from theory and experiment (Table S1); model test for Fe(110) on H_2O adsorption (Table S2); adsorption energies and structure parameters of the adsorbed species on Fe(110) surface (Table S3); adsorption energies and structure parameters of $(H_2O)_n$ clusters on Fe(110) surface(Table S4); adsorption energies and structure parameters of the IS, TS and FS for H_2O direct dissociation and $2H_2O$ dissociation on Fe(110) surface (Tables S5-S6); adsorption energies and bond distances of IS, TS and FS for the dissociations on Fe(110) surface (Tables S7-S8); optimized geometries for the stationary points of $2H_2O$ dissociation (Figures S1); optimized geometries for the stationary points of H_2O dissociation on nO pre-covered surface on Fe(110) surface (Figures S2-S9); potential energy surfaces for H_2O dissociation on nO(n = 2 - 8) pre-covered Fe(110) surface (Figures S10).

Table 1: Computed adsorption energies (E_{ads}, eV), Fe-X distances (d, Å; X = O, H, OH and OH_2) as well as the O-H distance and HOH angle (θ_{HOH}, degree) in the optimized water

	T-site	**LB**-site	**SB**-site	**3FH**-site
		H		
E_{ads}		-0.71 (-2.97[a])	-0.59 (-2.85[a])	-0.76 (-3.03[a])
	+0.06[5]	-0.63[5]	-0.51[5]	-0.69[5]
	(-2.28[41])	(-2.95[41])	(-2.81[41])	(-3.00[41])
	(-2.33[42])	(-2.76[42])	(-2.73[42])	(-2.71[42])
d_{H-Fe}		0.97[e] (1.75[f])	1.16[e] (1.70[f])	0.97[e] (1.79[f])
	1.52[5e]	0.94[5e]	1.16[5e]	0.95[5e]
	1.56[41e] (1.56[41f])	0.95[41e] (1.74[41f])	1.14[41e] (1.69[41f])	0.94[41e] (1.78[41f])
	1.46[42e] (1.36[42f])	0.89[42e] (1.69[42f])	1.03[42e] (1.61[42f])	0.87[42e] (1.74[42f])
		O		
E_{ads}	-1.77 (-5.19[b])	-3.43 (-6.84[b])	-2.94 (-6.35[b])	-3.43 (-6.84[b])
	-2.03[5]	-3.69[5]		
		-3.28[43]		
		-3.44[44]		
d_{O-Fe}	1.65[e] (1.65[f])	1.04[e] (1.85[f])	1.25[e] (1.85[f])	1.05[e] (1.85[f])
	1.69[43]	1.03[43e]		
		OH		
E_{ads}	-3.45		-3.95	-4.28
	-3.19[5]	-4.05[5]	-3.74[5]	
d_{O-Fe}	1.78		1.50[e] (1.93[f])	1.30[e] (2.00[f])
	1.95[5]	1.30[5e]	1.53[5e]	
d_{O-H}	0.97		0.97	0.98
	0.99[5]	1.00[5]	1.00[5]	
		OH_2		
E_{ads}	-0.38[c]		-0.28[d]	
	-0.26[5c]			
d_{O-Fe}	2.18[c]		2.36[d]	
	2.29[5c]			
d_{O-H}	0.98[c]		0.98[d]	
	1.01[5c]			
ϑ_{HOH}	106.0[c]		109.1[d]	
	112.1[5c]			

(a) Referencing to hydrogen atom in parenthesis. (b) Referencing to oxygen atom in parenthesis. (c) For titled adsorption configuration to the surface. (d) For perpendicular configuration to the surface in parenthesis. (e) Species-surface distance. (f) Distance from species to the nearest Fe atom.

Figure 1: Top (a) and side (b) views of the Fe(110) surface structures with possible adsorption sites: on-top (**T**), long-bridge (**LB**), short-bridge (**SB**) and three-fold-hollow (**3FH**) as well as the most stable adsorption configuration and energy of H, O, OH and H_2O

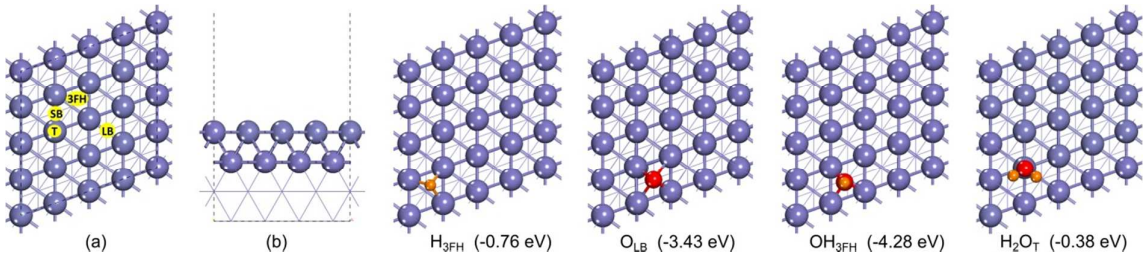

Figure 2. Most stable structures and the adsorption energy (eV) of $(H_2O)_n$ clusters on Fe(110) surface (iron/blue; oxygen/red; hydrogen/yellow; small oxygen atoms for shorter Fe-O distance and big oxygen atom for longer Fe-O distance)

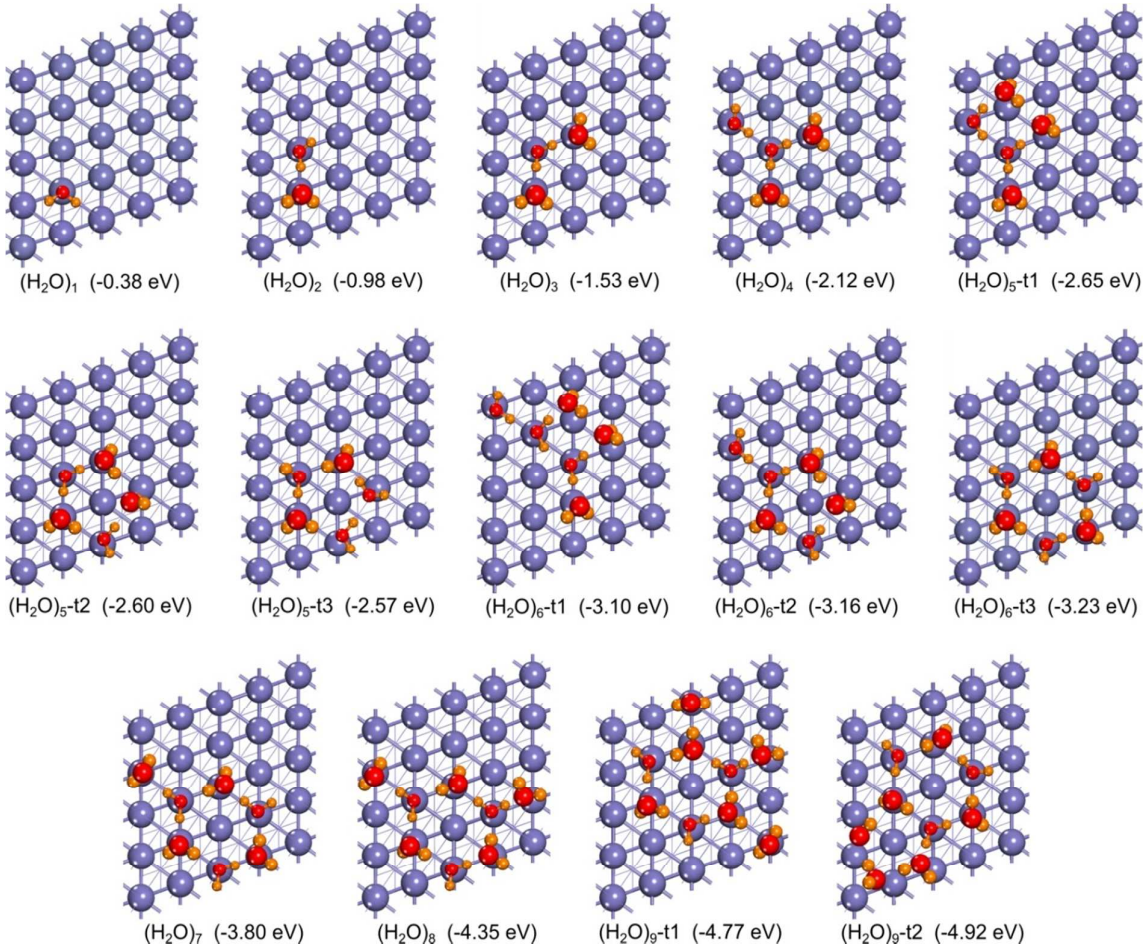

Figure 3: The optimized geometries and the adsorption energy (eV) for the stationary points in the reaction of H_2O direct dissociation on Fe(110) surface (iron/blue; oxygen/red; hydrogen/yellow)

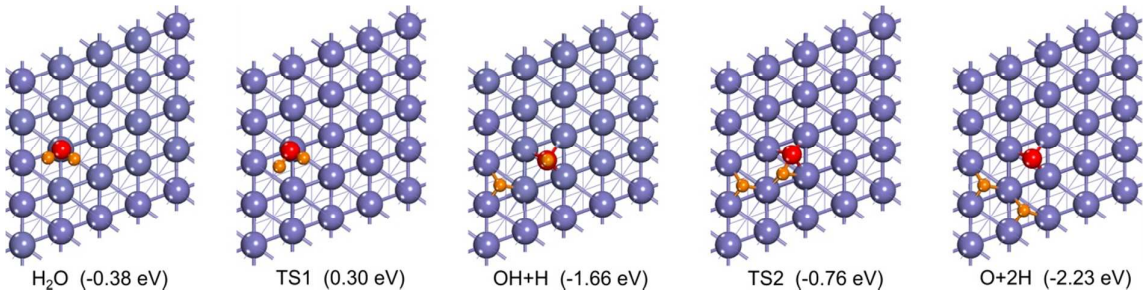

Figure 4: Potential energy surfaces (in eV) for the dissociation reaction of H_2O and $2H_2O$ on Fe(110) surface, as well as H_2O dissociation on *n*O pre-covered Fe(110) surface. The red data in the parentheses are the relevant reaction barriers (s for surface species; and g for gaseous species)

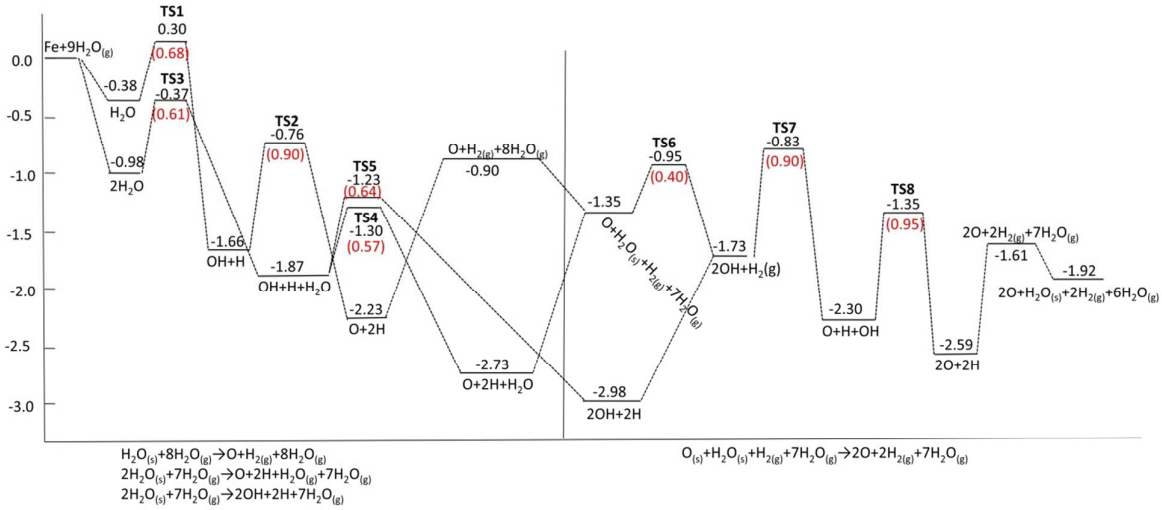

For the reaction, $nO+H_2O=(n+1)O+H_2$ from *n* = 2-6, the potential energy surfaces are similar as that for *n* = 1

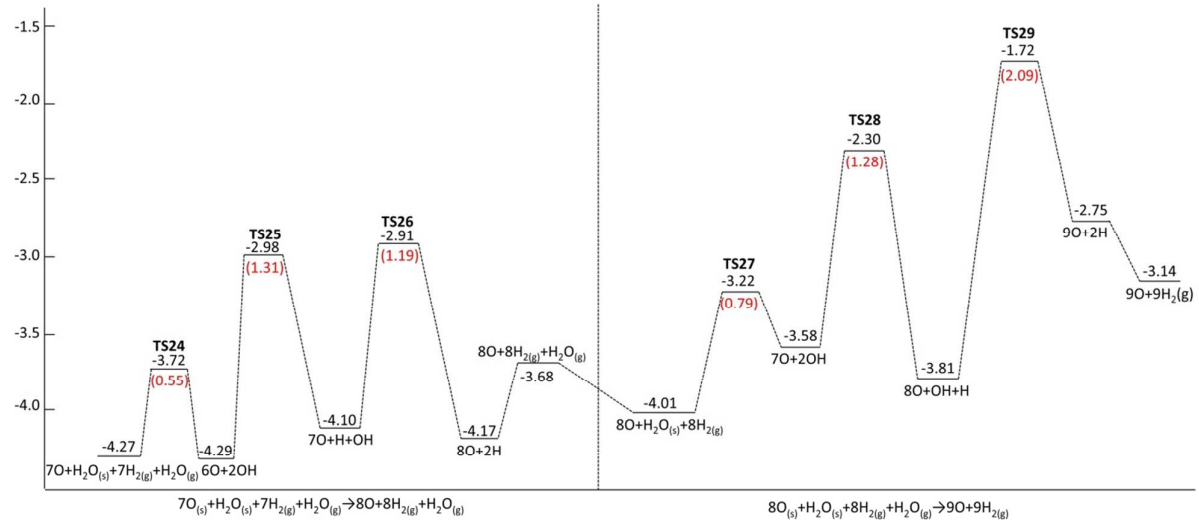

Figure 5. H_2O adsorption energy E_{ads} (eV), the barrier energies E_{a1} (eV) for nO+H_2O → (n-1)O+2OH; and E_{a2}, E_{a3} (eV) for the OH dissociation in the reactions of (n-1)O+2OH → nO+H+OH and nO+H+OH → (n+1)O+2H and H_2 desorption energies (E_{des}, eV) in the reaction of (n+1)O+2H →(n+1)O+H_2(g)

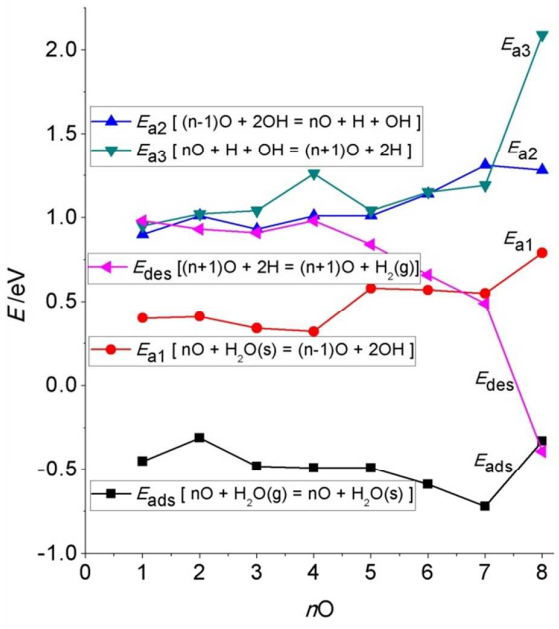

Figure 6. Geometries and adsorption energy (eV) of different ML of (a) OH and (b) O on Fe(110) surface. The structure of 6O+4OH+6H_2O is the optimized structure of 16OH, among the species, the smallest atoms (oxygen/red; hydrogen/light yellow) are the H_2O molecules adsorbing through the hydrogen bonding away from the surface. (iron/blue; oxygen/red; hydrogen/yellow)

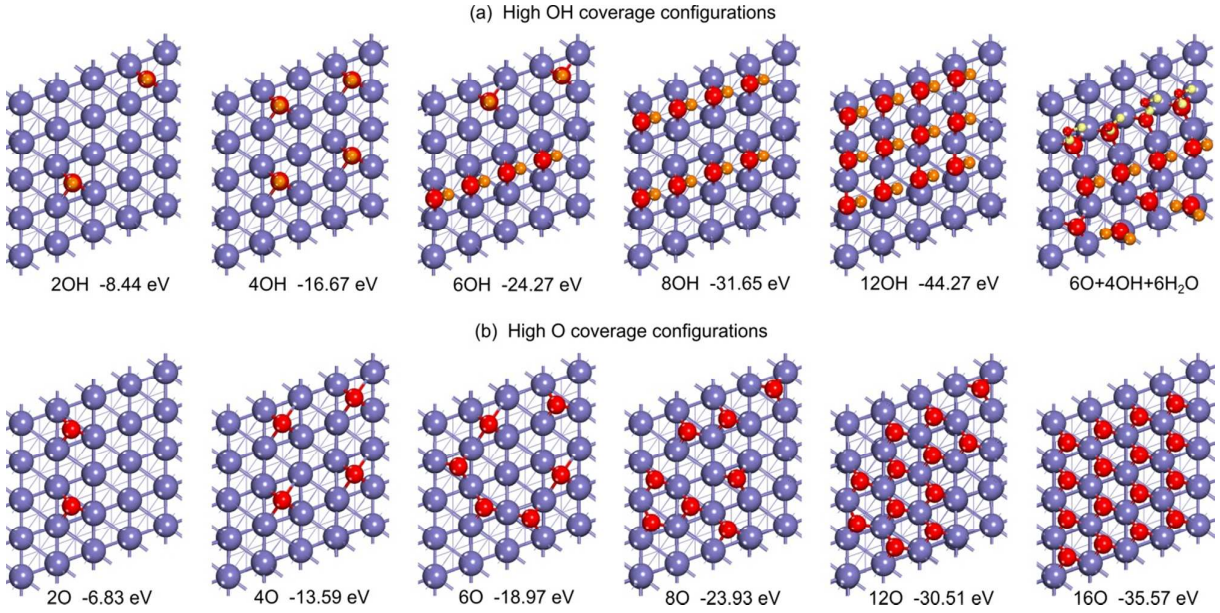

Figure 7. H_2O and H_2 desorption temperature under different conditions at 1.3×10^{-13} atmosphere on Fe(110) surface (s for surface species; and g for gaseous species)

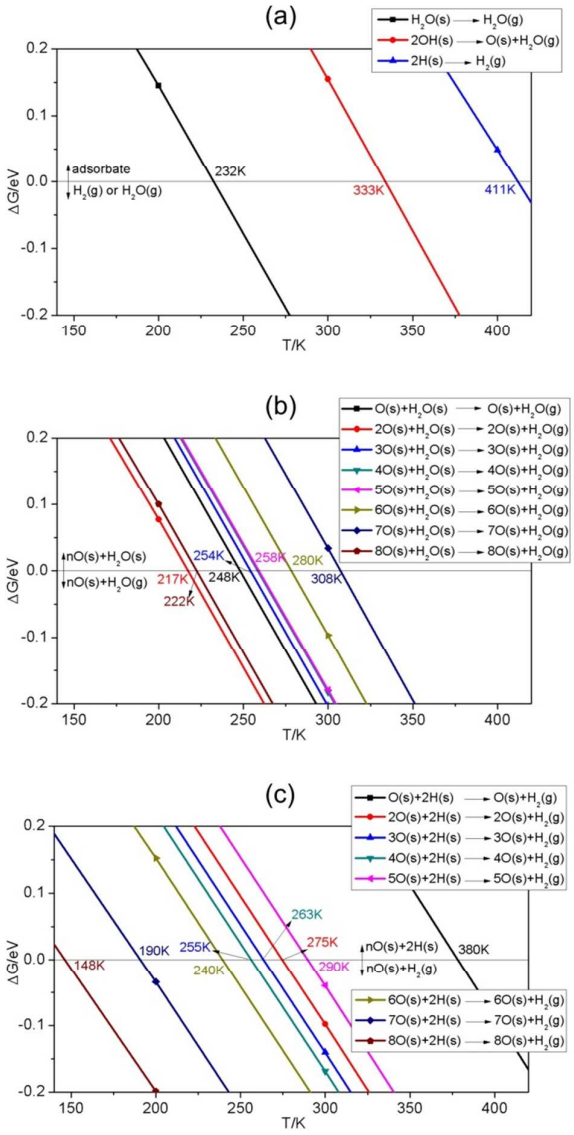

References

1 J.Carrasco, A. Hodgson and A. Michaelides, *Nature Materials* 2012, **11**, 667-674.

2 D. J. Dwyer, S. R. Kelemen and Kaldor, A. *J. Chem. Phys.* 1982, **76**, 1832-1837.

3 G. Pirug, G. Brodén and H. P. Bonzel, *Surf. Sci.* 1980, **94**, 323-338.

4 A. M. Baró and W. Erley, *J. Vas. Sci. Technol.* 1982, **20**, 580-583.

5 M. Eder and K. Terakura, *Phys. Rev. B* 2001, **64**, 115426.

6 A. B. Anderson, *Surf. Sci.* 1981, **105**, 159-176.

7 W. H. Hung, J. Schwartz and S. L. Bernasek, *Surf. Sci.* 1991**, 248**, 332-342.

8 W. H. Hung, J. Schwartz and S. L. Bernasek, *Surf. Sci.* 1993, **294**, 21-32.

9 D. E. Jiang and E. A. Carter, *J. Phys. Chem. B* 2004, **108**, 19140-19145.

10 J. M. H. Lo and T. Ziegler, *J. Phys. Chem. C* 2007, **111**, 11012-11025.

11 S. C. Jung and M. H. Kang, *Phys. Rev. B* 2010, **81**, 115460.

12 A. Govender, D. C. Ferré and J. W. Niemantsverdriet, *Chem. Phys. Chem.* 2012, **13**, 1583-1590.

13 R. R. Q. Freitas, R. Rivelino, F. de B. Mota and C. M. C. de. Castilho, *J. Phys. Chem. C* 2012, **116**, 20306-20314.

14 P. Lazar and M. Otyepka, *J. Phys. Chem. C* 2012, **116**, 25470-25477.

15 P. Błoński and A. Kiejna, *Vacuum* 2004, **74**, 179-183.

16 S. L. Liu, X. X. Tian, T. Wang, X. D. Wen, Y.-W. Li, J. Wang and H. Jiao, *J. Phys. Chem. C* 2014, **118**, 26139-26154.

17 G. Kresse and J. Furthmüller, *Comput. Mater. Sci.* 1996, **6**, 15 – 50.

18 G. Kresse and J. Furthmüller, *Phys. Rev. B: Condens. Matter* 1996, **54**, 11169 – 11186.

19 P. E. Blöchl, *Phys. Rev. B.* 1994, **50**, 17953-17979.

20 G. Kresse and D. Joubert, *Phys. Rev. B.* 1999, **59**, 1758 -1775.

21 J. P. Perdew, K. Burke and M. Ernzerhof, *Phys. Rev. Lett.* 1996, **77**, 3865 – 3868.

22 G.Henkelman, B. P. Uberuaga and H. Jónsson, *J. Chem. Phys.* 2000, **113**, 9901-9904.

23 H. J. Monkhorst and J. D. Pack, *Phys. Rev. B*. 1976, **13**, 5188-5192.

24 R. Kohlhaas, P. Donner and N. Schmitz-Pranghe, *Z. Angew. Phys.* 1967, **23**, 245.

25 C.Kittel, Introduction to Solid State Physics, 7th ed., Wiley, New York, 1996.

26 A.Hodgson and S. Haq, *Surf. Sci. Rep.* 2009, **64**, 381-451.

27 S. Grimme, *J. Comput. Chem.* 2006, **27**, 1787-1799.

28 E. R. McNellis, J. Meyer and K. Reuter, *Phys. Rev. B* 2009, **80**, 205414.

29 D. L. Chen, W. A. A. Saidi and J. K. Johnson, *J. Phys.: Condens. Matter.* 2012, **24**, 424211.

30 T. Bučko, J. Hafner, S. Lebègue and J. G. Ángyán, *J. Phys. Chem. A* 2012, **114**, 11814-11824.

31 T. Wang, X.-X. Tian, Y.-W. Li, J. Wang, M. Beller and H. Jiao, *ACS Catal.* 2014, **4**, 1991-2005.

32 T. Wang, S. Wang, Q. Luo, Y.-W. Li, J. Wang, M. Beller and H. Jiao, *J. Phys. Chem. C* 2014, **118**, 4181-4188.

33 R. Gao, D. B. Cao, S. L. Liu, J. Wang, Y. W. Li and H. Jiao, *Appl. Catal. A*. 2013, **468**, 370-384.

34 K.Reuter and M. Scheffler, *Phys. Rev. B* 2001, **65**, 035406.

35 K. Reuter and M. Scheffler, *Phys. Rev. B* 2003, **68**, 045407.

36 W. X. Li, C. Stampfl and M. Scheffler, *Phys. Rev .B* 2003, **68**, 165412.

37 F. Zasada, W. Piskorz, S. Cristol, J. F. Paul, A. Kotarba and Z. Sojka, *J. Phys. Chem. C* 2010, **114**, 22245-22253.

38 W. Piskorz, J. Gryboś, F. Zasada, P. Zapała, S. Cristol, J. F. Paul and Z. Sojka, *J. Phys. Chem. C* 2012, **116**, 19307-19320.

39 T. Wang, X. W. Liu, S. G. Wang, C. F. Huo, Y.-W. Li, J. Wang and H. Jiao, *J. Phys. Chem. C* 2011, **115**, 22360-22368.

40 T. Wang, S. G. Wang, Y. W. Li, J. Wang and H. Jiao, *J. Phys. Chem. C* 2012, **116**, 6340-6348.

41 D. E. Jiang and E. A. Carter, *Surf. Sci.* 2003, **547**, 85-98.

42 P. Cremaschi, H. Yang and J. L. Whitten, *Surf. Sci.* 1995, **330**, 255-264.

43 P. Błoński, A. Kiejna and J. Hafner, *Surf. Sci.* 2005, **590**, 88-100.

44 P. Błoński,; A. Kiejna and J. Hafner, *Phys. Rev. B*. 2008, **77**, 155424.